Inorg. Chem. **2008**, *47*, 7225−7232

Influence of the Apical Ligand in the Thermotropic Mesomorphism of Cationic Copper-Based Surfactants

Jeffery A. Driscoll,[†] Paul H. Keyes,[‡] Mary Jane Heeg,[†] Paul A. Heiney,[§] and Claudio N. Verani*[,†]

Department of Chemistry and Department of Physics and Astronomy, Wayne State University, Detroit, Michigan 48202, and Department of Physics and Astronomy, University of Pennsylvania, Philadelphia, Pennsylvania 19104

Received March 21, 2008

A new pyridine-based bidentate ligand L^{PyC18} was used to develop copper-containing surfactants that exhibit mesomorphism. Complexes $[(L^{PyC18})_2Cu^{II}Y]Y$ were synthesized, where Y is an anionic ligand bromo (**1**), nitrato (**2**), or perchlorato (**3**). The nature of these apical ligands determines the mesogenic behavior of **1**−**3**: The smallest bromo-substituted species **1** shows a metastable liquid crystalline phase at 110 °C, the nitrato-substituted **2** increases the transition temperature to 136 °C, and the bulky perchlorato-substituted **3** shows reversible mesophases at 153 °C. The behavior of these complexes shows similarities and suggests that at low temperatures the crystals of these compounds are bilayered structures with interdigitated alkyl tails. At higher temperatures the tails undergo rapid conformational changes that force these layers to swell until the opposing alkyl chains are separated from each other, and the mesophase is a monolayer smectic A. Small changes in the geometry of cationic mesogens can be imposed by the presence of apically coordinated anions, allowing for tuning in the properties of the resulting mesophases.

Introduction

Liquid crystalline mesogens are stimulus-responsive soft materials capable of forming well-defined structures. Current research encompasses applications well beyond their established role in information display technology, pointing toward nonconventional[1] systems that exhibit reflective,[2] luminescent,[3] and conductive[4] behavior. These properties are starting to be explored in the fabrication of protein-sensors,[5,6] photonic devices,[7] and molecular electronics.[8]

Cooperativity between metal ions and organic scaffolds leads to the incorporation of redox and magnetic properties,[9,10] as well as to the induction of macroscopic ordering in otherwise nonmesomorphic modules,[11] leading to new molecular architectures with distinctive organizations and tunable mesophases.[12–14] Controlled mono or dimeric copper centers,[15] uranium-based alaskaphyrins,[16] iron-tricarbollide derivatives,[17] and the inclusion of tridimensional μ-oxo-Cu_4

* To whom correspondence should be addressed. E-mail: cnverani@chem.wayne.edu. Phone: 313 577 1076. Fax: 313 577 8022.
[†] Department of Chemistry, Wayne State University.
[‡] Department of Physics and Astronomy, Wayne State University.
[§] Department of Physics and Astronomy, University of Pennsylvania.

(1) (a) Binnemans, K. *Chem. Rev.* **2005**, *105*, 4148. (b) Tschierske, C. *J. Mater. Chem.* **1998**, *8*, 1485. (c) Neve, F. *Adv. Mater.* **1996**, *8*, 277.
(2) Mitov, M.; Dessaud, N. *Nature Mater.* **2006**, *5*, 361.
(3) Camerel, F.; Bonardi, L.; Schmutz, M.; Ziessel, R. *J. Am. Chem. Soc.* **2006**, *128*, 4548.
(4) Woon, K. L.; Aldred, M. P.; Vlachos, P.; Mehl, G. H.; Stirner, T.; Kelly, S.; O'Neill, M. *Chem. Mater.* **2006**, *18*, 2311.
(5) Govindaraju, T.; Bertics, P. J.; Raines, R. T.; Abbott, N. L. *J. Am. Chem. Soc.* **2007**, *129*, 11223.
(6) Lockwood, N. A.; Cadwell, K. D.; Caruso, F.; Abbott, N. L. *Adv. Mater.* **2006**, *18*, 850.
(7) Urbas, A.; Tondiglia, V.; Natarajan, L.; Sutherland, R.; Yu, H.; Li, J.-H.; Bunning, T. *J. Am. Chem. Soc.* **2004**, *126*, 13580.
(8) Kadam, J.; Faul, C. F. J.; Scherf, U. *Chem. Mater.* **2004**, *16*, 3867; and references 1−12 therein.
(9) Binnemans, K.; Lodewyckx, K.; Donnio, B.; Guillon, D. *Chem.—Eur. J.* **2002**, *8*, 1101.
(10) Binnemans, K.; Galyametdinov, Y. G.; Van Deun, R.; Bruce, D. W.; Collinson, S. R.; Polishchuk, A. P.; Bikchantaev, I.; Haase, W.; Prosvirin, A. V.; Tinchurina, L.; Litvinov, I.; Gubajdullin, A.; Rakhmatullin, A.; Uytterhoeven, K.; Van, M. L. *J. Am. Chem. Soc.* **2000**, *122*, 4335.
(11) Camerel, F.; Ulrich, G.; Barbera, J.; Ziessel, R. *Chem.—Eur. J.* **2007**, *13*, 2189.
(12) Terazzi, E.; Suarez, S.; Torelli, S.; Nozary, H.; Imbert, D.; Mamula, O.; Rivera, J.-P.; Guillet, E.; Benech, J.-M.; Bernardinelli, G.; Scopelliti, R.; Donnio, B.; Guillon, D.; Bunzli, J.-C.; Piguet, C. *Adv. Funct. Mat.* **2006**, *16*, 157.
(13) Terazzi, E.; Torelli, S.; Bernardinelli, G.; Rivera, J.-P.; Benech, J.-M.; Bourgogne, C.; Donnio, B.; Guillon, D.; Imbert, D.; Buenzli, J.-C.; Pinto, A.; Jeannerat, D.; Piguet, C. *J. Am. Chem. Soc.* **2005**, *127*, 888.
(14) Date, R. W.; Iglesias, E. F.; Rowe, K. E.; Elliott, J. M.; Bruce, D. W. *Dalton Trans.* **2003**, 1914.

10.1021/ic8005162 CCC: $40.75
Published on Web 07/22/2008

Scheme 1. Cationic Surfactants

$[(L^{PY18})_2 Cu^{II} Br] Br$ (1)
$[(L^{PY18})_2 Cu^{II} NO_3] NO_3$ (2)
$[(L^{PY18})_2 Cu^{II} ClO_4] ClO_4$ (3)
$[(L^{PY14})_2 Cu^{II} Br] Br$ (4)
$[(L^{PY14})_2 Cu^{II} NO_3] NO_3$ (5)

clusters,[18] among many others, attest to the vitality of the field, whereas dynamic thermochromic,[19] ferroelectric,[20] and spin-crossover[21,22] materials point to its future. Such developments suggest that the inclusion of metallomesogenic materials in device development is eminent.

Of particular relevance to this work, small changes in the geometry of cationic mesogens can be imposed by the presence of anions, allowing for tuning of the resulting mesophases. This effect has been observed for cis-oriented counterions such as halogens and azides coordinated to square planar nickel, palladium, and platinum systems,[23] as well as for chlorides and nitrates coordinated to lanthanides.[24] In spite of these observations, the influence of the nature of the counterion serving as an apical ligand coordinated to the metal in the thermotropic mesomorphism of mesogens has not been extensively studied.

In this article we investigate five copper(II) compounds of formula $[(L^{PyCX})_2Cu^{II}Y]Y$ shown in Scheme 1. The ligand L^{PyCX}, originally designed as an end-capping amphiphile for iron(III) molecular switches,[25,26] is a substituted aminomethylpyridine in which CX designates the length of the alkyl chain. Complexes **1**, **2**, and **3** display $CX = C_{18}H_{37}$, whereas a $C_{14}H_{29}$ chain is present in complexes **4** and **5**. The apically coordinated species Y^- is an anionic ligand such as a bromo (Br^-), perchlorato (ClO_4^-), or nitrato (NO_3^-). An uncoordinated counterion is also present for charge balance. We present the syntheses, characterization, and detailed study of the structural features of the solids, as well as their distinctive mesomorphic properties confirmed by differential scanning calorimetry (DSC), polarized optical microscopy, and X-ray diffraction. We conclude with a rationale about the role of the apical ligands and the advantages and the limitations of the approach.

Experimental Section

Materials and Methods. All reagents were used as received from commercial sources. Methanol was dried using calcium hydride, and dichloromethane was doubly purified using alumina columns in an Innovative Technologies solvent purification system. Infrared spectra were measured from 4000 to 400 cm^{-1} as KBr pellets on a Bruker Tensor 27 FTIR spectrophotometer. ^1H NMR spectra were measured using a Varian 400 MHz instrument. ESI (positive) spectra were measured in a Micromass Quattro LC triple quadrupole mass spectrometer, and experimental assignments were simulated for peak position and isotopic distribution. Elemental analyses were performed by Midwest Microlab in Indianapolis, Indiana.

Molecular Structural Determination. Diffraction data were measured on a Bruker X8 APEX-II kappa geometry diffractometer with Mo radiation and a graphite monochromator. Frames were collected at 100 K with the detector at 40 mm and 0.3−0.5 degrees between each frame and were recorded for 10−20 s. APEX-II and SHELX-97 software packages[27,28] were used in the collection and refinement of the models. Crystals of $[(L^{PyC18})_2Cu^{II}ClO_4]ClO_4$ **(3)** appeared as purple plates, and the fragment size was 0.15 × 0.12 × 0.04 mm^3. A total of 43 568 reflections were recorded, of which 12 724 were unique. Both pendant arms of the complex showed disorder. One arm was more severely disordered, and partial atomic positions were assigned and kept isotropic. Some atoms in the octadecyl (C_{18}) chain were less severely disordered but resulted in unreliable bond lengths within the chain because of the inability to assign partial atoms with very close displacements. Hydrogen bonds exist between N−H and the perchlorato oxygens. The asymmetric unit contains one copper complex and two perchlorate anions. Crystals of $[(L^{PyC14})_2Cu^{II}Br]Br$ **(4)** were blue rods or plates; the diffraction sample was 0.26 × 0.15 × 0.10 mm^3. A total of 45 553 reflections were recorded, yielding 10 768 independent *hkl* data. One of the dangling arms of the ligand was severely disordered and described as two chains of half-occupancy and held isotropic. Bond lengths in the disordered chain were constrained to 1.54 Å during refinement. Both amine hydrogen atoms are engaged in hydrogen bonds to Br atoms. The asymmetric unit consists of one copper complex and one bromide anion with no solvent. Complex $[(L^{PyC14})_2Cu^{II}NO_3]NO_3$ **(5)** crystallized as blue flat rods. The mounted sample was 0.17 × 0.16 × 0.08 mm^3. A total of 58 689 data points were integrated and averaged to yield 10 814 independent reflections. The tetradecyl (C_{14}) arms of the ligand were ordered. One nitrate is O-bound to the copper, and one is a counterion in the lattice. Both nitrates show hydrogen bonds to the amine hydrogens. The asymmetric unit contains one copper complex and one NO_3^- anion. In all cases hydrogen atoms were placed in calculated positions. Crystal data for all three compounds are summarized in Table 1.

Polarized Optical Microscopy. Observations of the samples were performed on the stage of a Nikon Labphot polarizing

(15) Elliott, J. M.; Chipperfield, J. R.; Clark, S.; Teat, S. J.; Sinn, E. *Inorg. Chem.* **2002**, *41*, 293.
(16) Sessler, J. L.; Callaway, W. B.; Dudek, S. P.; Date, R. W.; Bruce, D. W. *Inorg. Chem.* **2004**, *43*, 6650.
(17) Januszko, A.; Kaszynski, P.; Grüner, B. *Inorg. Chem.* **2007**, *46*, 6078.
(18) Shakya, R.; Keyes, P. H.; Heeg, M. J.; Moussawel, A.; Heiney, P. A.; Verani, C. N. *Inorg. Chem.* **2006**, *45*, 7587.
(19) Seredyuk, M.; Gaspar, A. B.; Ksenofontov, V.; Reiman, S.; Galyametdinov, Y.; Haase, W.; Rentschler, E.; Guetlich, P. *Chem. Mater.* **2006**, *18*, 2513.
(20) Serrano, J. L.; Sierra, T. *Chem.—Eur. J.* **2000**, *6*, 759.
(21) Hayami, S.; Motokawa, N.; Shuto, A.; Masuhara, N.; Someya, T.; Ogawa, Y.; Inoue, K.; Maeda, Y. *Inorg. Chem.* **2007**, *46*, 1789.
(22) Zhang, W.; Zhao, F.; Liu, T.; Yuan, M.; Wang, Z. M.; Gao, S. *Inorg. Chem.* **2007**, *46*, 2541.
(23) Pucci, D.; Barberio, G.; Crispini, A.; Francescangeli, O.; Ghedini, M.; La, D. M. *Eur. J. Inorg. Chem.* **2003**, *19*, 3649.
(24) Binnemans, K.; Moors, D.; Parac, V.; Tatjana, N.; Van, D. R.; Hinz, H. D.; Meyer, G. *Liq. Cryst.* **2002**, *29*, 1209.
(25) Lanznaster, M.; Hratchian, H. P.; Heeg, M. J.; Hryhorczuk, L. M.; McGarvey, B. R.; Schlegel, H. B.; Verani, C. N. *Inorg. Chem.* **2006**, *45*, 955.
(26) Lanznaster, M.; Heeg, M. J.; Yee, G. T.; McGarvey, B. R.; Verani, C. N. *Inorg. Chem.* **2007**, *46*, 72.
(27) *APEX II collection and processing programs*; Bruker AXS Inc.: Madison, WI.
(28) Sheldrick, G. M. *SHELXL93. University of Göttingen*: Göttingen, Germany, 1997.

Table 1. Crystal Data for **3**, **4**, and **5**

	$(L^{PyC18})_2Cu^{II}ClO_4]ClO_4$ (**3**)	$[(L^{PyC14})_2Cu^{II}Br]Br$ (**4**)	$[(L^{PyC14})_2Cu^{II}NO_3]NO_3$ (**5**)
formula	$C_{48}H_{88}Cl_2CuN_4O_8$	$C_{40}H_{72}Br_2CuN_4$	$C_{40}H_{72}CuN_6O_6$
fw	983.66	832.38	796.58
space group	triclinic, $P\bar{1}$	triclinic, $P\bar{1}$	triclinic, $P\bar{1}$
a (Å)	9.9383(4)	9.468(1)	9.5722(2)
b (Å)	11.8276(5)	11.236(1)	11.6249(3)
c (Å)	23.9031(1)	21.837(2)	21.4333(5)
α (deg)	90.810(2)	91.890(5)	79.767(1)
β (deg)	98.506(3)	96.216(5)	78.7590(1)
γ (deg)	110.466(2)	109.454(5)	69.376(1)
V (Å^3)	2596.8(2)	2171.7(4)	2173.85(9)
Z	2	2	2
temp (K)	100(2)	100(2)	100(2)
λ (Å)	0.71073	0.71073	0.71073
density, (g cm^{-3})	1.258	1.273	1.217
μ (mm^{-1})	0.576	2.373	0.552
$R(F)$ (%)[a]	4.91	7.62	4.52
$Rw(F)$ (%)[a]	12.01	18.89	9.36

[a] $R(F) = \sum||F_o| - |F_c||/\sum|F_o|$ for $I > 2\sigma(I)$; $Rw(F) = \sum w(F_o^2 - F_c^2)^2/\sum w(F_o^2)^2]^{1/2}$ for $I > 2\sigma(I)$.

microscope. The field of view presented in the micrographs is approximately 1 × 1 mm, and the sample temperatures were maintained using a Mettler FP82 hot stage controlled by a Mettler FP80 central processor.

Mesophase X-ray Diffraction. Small-angle X-ray scattering measurements of the mesophase structures of **1**, **2**, and **3** employed a Bruker-Nonius FR591 rotating-anode generator with a copper anode operated at 3.4 kW. The beam was collimated and focused with mirror-monochromator optics, and the scattered radiation was detected using a Bruker Hi-Star wire (area) detector.[29] Samples were sealed in 1 mm diameter glass capillaries. Measurements were made in two configurations: at a fixed sample−detector distance of 54 cm ("intermediate angle") which probed *d*-spacings in the range of 1.6 to 16.0 nm, and a sample−detector distance of 11 cm ("wide angle") which probed *d*-spacings in the 0.37−3.0 nm range. In-situ temperature-dependent measurements employed a custom Linkam heating cell with an absolute temperature accuracy of ±5 °C. Primary data analysis was performed using Datasqueeze.[30]

Differential Scanning Calorimetry. Samples were analyzed using a TA Instruments Q1000 differential scanning calorimeter. A linear heating rate of 10 °C/min was applied to all samples, and a few milligrams of sample were used for each analysis. An indium standard was used for temperature calibration.

Synthesis of the Ligands. Octadecylamine (2.69 g, 10.0 mmol) or tetradecylamine (2.13 g, 10.0 mmol) were dissolved in 100 mL of MeOH and treated with pyridine-carboxyaldehyde (1.07 g: 10.0 mmol) under mild heat for 4 h. The resulting Schiff-base was reduced with $NaBH_4$ at 0 °C. The solution was stirred for 3 h, followed by solvent removal. The crude product was dissolved in CH_2Cl_2 and washed several times in a 5% Na_2CO_3 aqueous solution in a separation funnel. The resulting amines were dried over Na_2SO_4 for 24 h and recrystallized in acetone at 0 °C. Characterizations are as follows:

Octadecyl-pyridin-2-ylmethyl-amine, L^{PyC18}. Yield 81%. IR (KBr, cm^{-1}) 2920(s), 2850(s) (alkyl- CH_2-); 1134(m) (R′-NH-R); 1349(m) ($CH_{aromatic}$); 1592(vs), 1564(m), 1467(vs) (C═N_{pyr}) and (C═C); ^{1}H NMR data [400 MHz, $CDCl_3$, 300 K δ (ppm): 0.85 [t, CH_3], 1.16−1.23 [overlapped m, 30H (CH_2)], 1.48 [t, NCH_2CH_2-], 2.62 [t, -CH_2NH-], 3.88 [s, -NCH_2-Py)]; 7.12 [d, 1H (Py)], 7.26 [t, 1H (Py)], 7.58 [t, 1 H (Py)], 8.52 [d, 1 H (Py)]. ESI Pos. in MeOH *m/z*: 361.29 for $[L^{PyC18} + H^+]^+$.

Tetradecyl-pyridin-2-ylmethyl-amine, L^{PyC14}. Yield 82%. IR (KBr, cm^{-1}) 2924(s), 2852(s) (alkyl- CH_2-); 1590 (vs) 1570(m), 1467(vs) (C═N_{pyr}) and (C═C); 1127(m) (R′-NH-R); 1377(m) ($CH_{aromatic}$); ^{1}H NMR data [400 MHz, $CDCl_3$, 300 K δ (ppm): 0.87 [t, CH_3], 1.02−1.24 [overlapped m, 22 (CH_2)], 1.53 [t, NCH_2CH_2-], 2.64 [t, -CH_2NH-], 3.90 [s, -NCH_2-Py)]; 7.15 [d, 1H (Py)], 7.28 [t, 1H (Py)], 7.62 [t, 1 H (Py)], 8.54 [d, 1 H (Py)] ESI Pos. in MeOH *m/z*: 305.3 for $[L^{PyC14} + H^+]^+$.

Synthesis of the Complexes. Caution! *Complex* **3** *is a perchlorate salt and therefore potentially explosive. Small amounts of material should be used for synthesis and analyses and proper safety precautions should be taken.*

Complexes **1**−**5** were synthesized by dissolving 2.5 mmol of the appropriate ligand (L^{PyC18} or L^{pyC14}) in 25 mL of MeOH and adding it dropwise to a 10 mL of MeOH solution containing $CuBr_2$ for **1** and **4**, $Cu(NO_3)_2 \cdot 3H_2O$ for **2** and **5**, or $Cu(ClO_4)_2 \cdot 6H_2O$ for **3**. The 2:1 ligand to metal ratio mixture was stirred under a mild reflux for 3 h. Complexes **2**, **3**, and **5** precipitate after removal of two-thirds of solvent volume by rotoevaporation, whereas **1** and **4**, are crashed with small amounts of dichloromethane. All species were isolated by vacuum filtration, and the resulting microcrystalline powders were recrystallized in suitable 1:1 solvent mixtures. X-ray quality crystals were isolated in MeCN/$CHCl_3$ for **3**, EtOH/$CHCl_3$ for **4**, and iPrOH/$CHCl_3$ for **5.** Characterizations are as follows:

$[(L^{PyC18})_2Cu^{II}Br]Br$ (1). Yield = 84%. Anal. Calcd for $C_{48}H_{88}Br_2CuN_4$: C, 61.03; H, 9.31; N, 5.93%. Found: C, 60.81; H, 8.96; N 5.91%. IR (KBr, cm^{-1}) 2849(s), 2918(s) (alkyl- CH-); 1364 (C═$N_{aromatic}$); 1148(s) (R′-NH-R); 1609(s), 1570(m), 1468(m) (C═N_{pyr}) and (C═C); ESI Pos. in MeOH: *m/z* (100%) = 864.7 for $[(L^{PyC18})_2Cu^{II}Br]^+$. Mp = 134−135 °C.

$[(L^{PyC18})_2Cu^{II}NO_3]NO_3$ (2). Yield = 84%. Anal. Calcd for $C_{48}H_{90}CuN_6O_6$: C, 63.44; H, 9.76; N, 9.25%. Found: C, 63.81; H, 9.28; N 9.15%. IR (KBr, cm^{-1}) (R′-NH-R); 2847(s), 2914(s) (alkyl- CH-); 1430(m) (CH_2CH_2); 1609(s) 1476(m) (C═N_{pyr}) and (C═C); 1405(s), 1340(s), 1305(s) (NO_3^-); ESI Pos. in MeOH: *m/z* (100%) = 845.62 for $[(L^{PyC18})_2Cu^{II}NO_3]^+$. Mp = 152−154 °C.

$[(L^{PyC18})_2Cu^{II}ClO_4]ClO_4$ (3). Yield = 87%. Anal. Calcd for $C_{48}H_{88}Cl_2CuN_4O_8$: C, 58.61; H, 9.02; N, 5.70%. Found: C, 58.31; H, 8.82; N 5.70%. IR (KBr, cm^{-1}) 2919(s), 2850(s) (alkyl- CH-); 1486(m) (CH_2CH_2); 1613(s), 1574(m), 1486(m) (C═N_{pyr}) and

(29) For additional details, see http://www.lrsm.upenn.edu/lrsm/facMAXS.html.
(30) For additional details, see http://www.datasqueezesoftware.com.

(C═C); 1574(s) (R′-NH-R); 1108(m), 1063(m), 1043(m), 624(s) (ClO_4^-); ESI Pos. in MeOH: *m/z* (100%) = 882.58 for $[(L^{PyC18})_2Cu^{II}ClO_4]^+$. Mp = 152−154 °C.

$[L^{PyC14})_2Cu^{II}Br]Br$ (4). Yield = 79%. Anal. Calcd for $C_{40}H_{72}Br_2CuN_4$: C, 57.72; H, 8.72; N, 6.73%. Found: C, 57.78; H, 8.74; N 6.69%. IR (KBr, cm^{-1}) 2847(s), 2920(s) (alkyl- CH_2-); 1607(s), 1570(m), 1467(m) (C═N_{pyr}) and (C═C); 1148(s) (R′-NH-R); ESI Pos. in MeOH: *m/z* (100%) = 750.4 for $[(L^{PyC14})_2Cu^{II}Br]^+$. Mp = 142−144 °C.

$[L^{PyC14})_2Cu^{II}NO_3]NO_3$ (5). Yield = 83%. Anal. Calcd for $C_{40}H_{72}CuN_6O_6$: C, 60.31; H, 9.11; N, 10.55%. Found: C, 59.94; H, 8.92; N 10.41%. IR (KBr, cm^{-1}) 2850(s), 2918(s) (alkyl- CH-); 1472(m) 1480(m) (pyr- CH═CH); 1155(m) (R′-NH-R); 1612(s), 1467(m) (C═N_{pyr}) and (C═C); 1411(s) 1331(m) 1308(s) (NO_3^-); ESI Pos. in MeOH: *m/z* (100%) = 733.5 for $[L^{PyC14})_2Cu^{II}NO_3]^+$. Mp = 149−151 °C.

Results and Discussion

Synthesis and Characterization of the Ligands. Schiff base condensation of 2-pyridinecarboxyaldehyde with 1-octadecylamine or 1-tetradecylamine in methanol gave the equivalent imine that was reduced in presence of $NaBH_4$ yielding the chelating surfactants octadecyl-pyridin-2-ylmethyl-amine $L^{Py18}$and tetradecyl-pyridin-2-ylmethyl-amine L^{Py14} with overall yields of 78−84%. The ligands were fully characterized by ^1H NMR, ESI mass spectrometry, and IR spectroscopy. The ESI^+ mass analyses showed peaks with *m/z* = 361.3 for $[L^{Py18} + H^+]^+$ and 305.2 for $[L^{Py14} + H^+]^+$. Peak simulation showed excellent agreement between position and isotopic distributions. The IR data showed peaks at 1590, 1570, 1467 cm^{-1} assigned to the stretching vibration of the aromatic C═Npy and C═C bonds and in the 2920 to 2850 cm^{-1} range, associated with the typical alkyl vibrations. The amine nature of the ligands was indicated by peaks at 3303 cm^{-1} for CH_2-NH-py. The ^1H NMR data also showed the corresponding protons as expected from the combined C−H groups from the pyridine and the alkyl chains.

Synthesis and Characterization of the Complexes. Treatment of the ligands with copper(II) salts yielded complexes **1** to **5** in 2:1 ligand to metal ratio. These complexes were fully characterized by IR spectroscopy, ESI^+ mass spectrometry, and elemental analyses. Upon coordination, the aromatic C═Npy and the secondary amino group peaks are shifted to lower frequencies suggesting that the electronic density of the bonds have increased.[31] The Cu−Br peaks for **1** and **4** fall outside of the detection range of the instrument. Nonetheless, data indicate the presence of distinct coordination modes in the nitrate ions of **2** and **5** and the perchlorate ions of **3**. Peaks arising from metal-bound nitrate are observed at about 1308 cm^{-1}, whereas those at 1411 and 1331 cm^{-1} are typical for the free counterion. Similarly, the peak at about 1043 cm^{-1} is typical for the free perchlorate, whereas those at 1108 and 1063 relate to peaks arising from the metal-bound ions.[32] Another peak at 624 cm^{-1} was also present for the perchlorate ions. Taking into account the denticity of the ligands and the favored five-coordination of a $3d^9$ ion, this result suggests that nitrates and perchlorates (and possibly bromides) are apically bound to a five coordinated bivalent copper ion. Further evidence comes from ESI(pos) mass spectrometry in which *m/z* peak clusters were observed for the equivalent $[L^{PyC18})_2Cu^{II}X]^+$ cations for **1** to **5**. Besides copper, isotopic distributions are in good agreement with the presence of ^{79}Br (50.69%) and ^{81}Br (40.61%) for **1** and **4.** All elemental analyses are in good agreement with the expected calculated values. On the basis of the data above, it can be inferred that the cations of complexes **1** to **5** are formed by two ligands coordinated to the copper center and that a charged anion (Br^-, NO_3^-, or ClO_4^-) must be coordinated as an apical ligand. An uncoordinated anion must be present for charge balance.

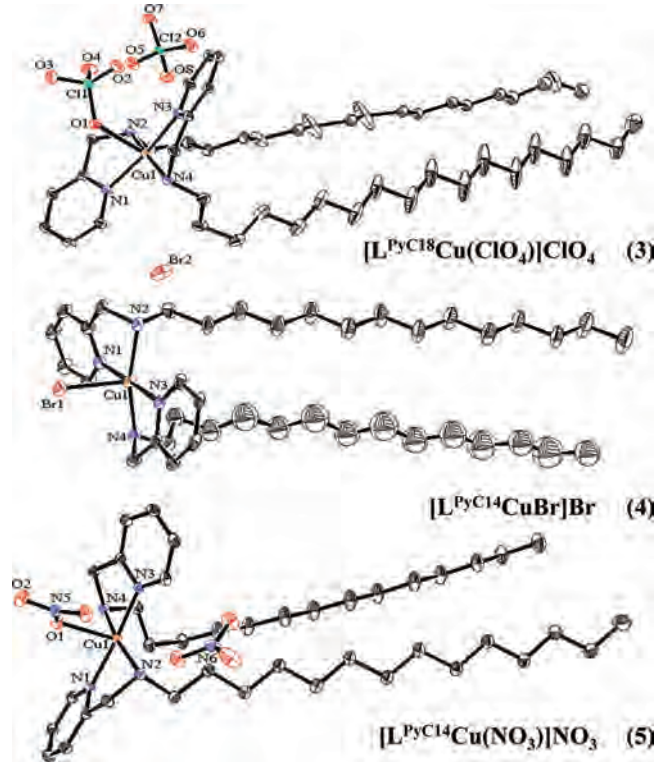

Figure 1. ORTEP drawing at the 40% probability level for the cations of **3**, **4**, and **5**. The cationic species are formed of two ligands coordinated to the copper center and an apically coordinated anion. Selected bond lengths (A) for **3**: Cu−N(pyr) = 2.010(2) and 2.002(2); Cu−N(amine) = 2.015(2) and 2.020(2); Cu−O = 2.495(2). For **4**: Cu−N(pyr) = 2.036(4) and 2.019(4); Cu−N(amine) = 2.026(4) and 2.015(4); Cu−Br = 2.761(1). For **5**: Cu−N(pyr) = 2.008(2) and 2.003(2); Cu−N(amine) = 2.015(2) and 2.011(2); Cu−O = 2.367(1).

Molecular Structures. The molecular structure of **3** was determined by X-ray crystallography of single crystals at 100 K obtained from slow evaporation of 1:1 ethanol/chloroform mixtures. Several attempts to obtain X-ray quality crystals for **1** and **2** failed. To infer structural information for these species, ligand L^{Py14} was used yielding **4** and **5**. These species are expected to serve as accurate models for **1** and **2**. The Oak Ridge Thermal Ellipsoid Plot (ORTEP) diagrams for the compounds **3**, **4**, and **5** are depicted in Figure 1 with selected bond lengths provided in the caption.

Complex **3** crystallizes with an asymmetric unit containing the cationic complex and a perchlorate anion with no solvent

(31) Valencia, L.; Bastida, R.; Fernandez-Fernandez, M. del C.; Macias, A.; Vicente, M. *Inorg. Chim. Acta* **2005**, *358*, 2618.
(32) Nakamoto, K. *Infrared and Raman Spectra of Inorganic and Coordination Compounds*, 5th ed.; Wiley-Interscience: New York, 1997.

in the lattice. The cation core is an N_4CuO species, with the perchlorato ligand bound to copper through oxygen with a typical Cu−O length.[33] The bite angles at copper of the amine and pyridine nitrogen atoms from the same ligand are 81.34(8) and 81.70(8) °. The N−Cu−N trans basal angles in the core are 171.53(9) and 170.36(9) °, yielding $\tau = 0.02$ in line with the expected value for a square-pyramidal geometry around Cu(II) complexes.

Complexes **4** and **5** were obtained with the ligand L^{Py14} aiming at the modeling of **1** and **2**. These are structurally related showing the same 2:1 ligand to metal stoichiometry for the complex cation and the presence of one lattice anion (bromide for **1** and **4** and nitrate for **2** and **5**, respectively) for charge balance. Complex **5** is very similar to **3** in the core structure. The ligand bite angles in **5** are 81.06(6) and 81.15(7)°. The N−Cu−N trans angles are 174.60(6) and 166.77(7)°. The Cu−N bond lengths are comparable between **3** and **5**. The tau value in **5** ($\tau = 0.13$) indicates a slightly more distorted square pyramidal coordination mode than that in **3** ($\tau = 0.02$). Complex **4** shows a definite impact from the Br donor. Ligand bite angles are 80.45(2) and 81.8(2)°, and the N−Cu−N trans angles are 179.0(2) and 161.4(2)°, yielding $\tau = 0.3$. Furthermore, the Cu−N(pyr) lengths in **4** are significantly longer than those observed in **3** and **5** (cf. average Cu−N(pyr) = 2.006 in **3**, 2.006 in **5**, and 2.028 in **4**).

The coordination sphere around copper (II) in these complexes is illustrating steric effects resulting from the apical ligand. With the perchlorato in **3**, nitrato in **5**, and bromo in **4** ligands the τ-values are $0.02 < 0.13 < 0.30$, and the square pyramidal geometries range from near perfect to heavily distorted. Compounds **3**, **4**, and **5** show a trans orientation of the pyridine rings within the same molecule and lack any kind of perpendicular overlap and ring stacking in vicinal molecules.

To analyze the thermotropic properties of the mesophases, it is fundamental to have an understanding of the molecular arrangement, as well as of the extended order and periodicity in the crystalline solids. The structures of **3**, **4**, and **5** show a lamellar nature in which the copper-containing head groups of vicinal cations are arranged face-on in close proximity along with the uncoordinated counterions. This organization in lamellar planes is held by strong ionic interactions and hydrogen bonds, as well as weaker dipole−dipole interactions, and is believed to allow the structures to slide past one another in a glide plane when in the liquid crystalline phases. The alkyl chains are interdigitated in an end-on fashion and form a secondary lamellar arrangement supported by weak van der Waals forces, as shown in Figure 2. The relative position of the head groups—and therefore the nature of the anionic ligands—influences the orientation of the chains. Complexes **3**, **4**, and **5** show an alternating pattern in the arrangement of their alkyl chains.

Polarized Optical Microscopy. The phase behavior presented by each of these compounds is complex, varied, and markedly history dependent. Not all of the phase

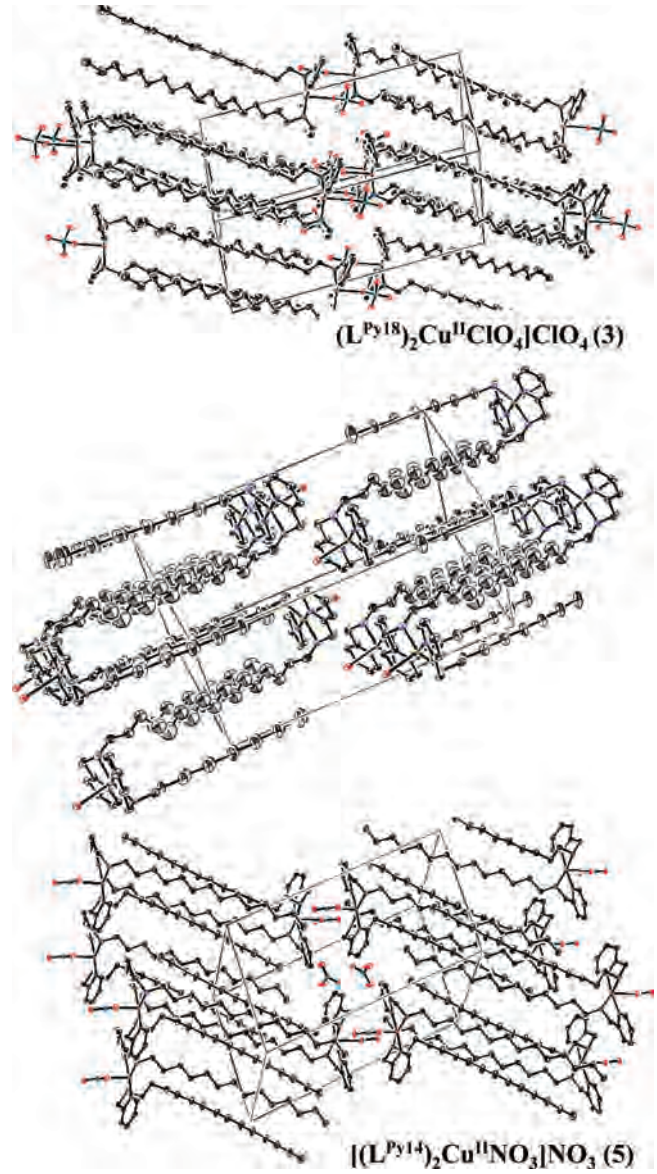

Figure 2. Unit cells for **3**, **4**, and **5**.

transitions revealed by DSC and X-ray diffraction were observed via polarized optical microscopy. Normally only one crystalline phase was observed. Even when multiple phases were detected and are known to be present, a single liquid crystalline phase was observed, followed by the high temperature isotropic liquid phase. However, the changes between the solid crystalline phase, the liquid crystalline phase, and the isotropic liquid were distinctly differentiated when observed through crossed polarizers. As expected, the isotropic liquid was characterized by a black texture related to a lack of birefringency. The solid crystal and the liquid crystal, both being birefringent, were bright and easily distinguished from each other by their different textures. In addition, in these metal-containing compounds and unlike other mesogenic compounds, the crystal and the liquid crystal generally had a very different predominant color.

The bromo-containing complex **1** was observed to melt from a crystalline phase to an isotropic liquid at 127 °C. Upon cooling, the compound underwent a monotropic transition to a metastable liquid crystal at 110 °C. A polarized

(33) Holmes, R. R. *J. Am. Chem. Soc.* **1984**, *106*, 3745.

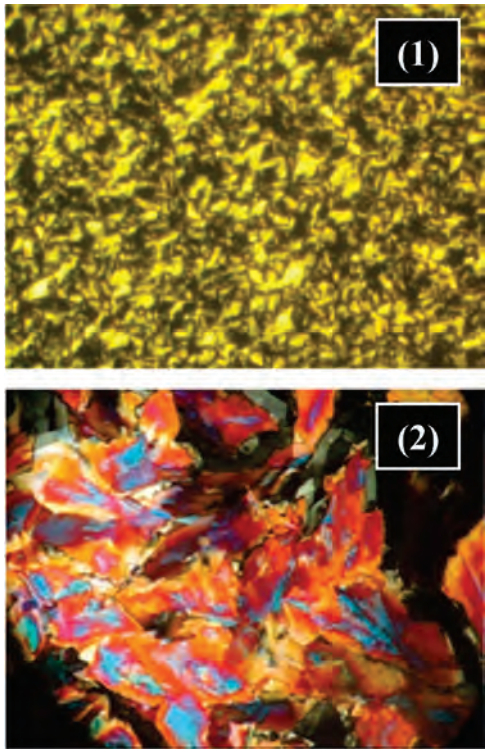

Figure 3. Micrographs of the liquid crystalline phases for **1** at 110 °C (top) and **2** at 136 °C (bottom).

micrograph of the liquid crystal is shown in Figure 3 top. It appears to have a focal conic texture like that of a smectic A liquid crystal. Similar phases have been reported in recent years for a number of four-coordinate copper mesogens with naphthylamine,[34] enaminoketone,[35] salycilaldimine,[36,37] cholesterol,[38] and tetrazole[39] ligands.

The nitrato-containing complex **2** was also observed to have metastable liquid crystalline phase. It melted from a crystal to the isotropic liquid at 142 °C, and on cooling a liquid crystal appeared at 136 °C (Figure 3 bottom). This mesophase remained stable down to 81 °C, at which point it began to crystallize. The texture of this liquid crystalline phase is quite different from that of complex **1**. It is very much like that of complex **3**, discussed below, but less bright and therefore somewhat less distinct. The similarity between complexes **2** and **3** can be attributed to the fact that both systems exhibit a bulky oxoanion coordinated to copper in the apical position.

The perchlorato-containing complex **3** is the only one of the studied compounds to have a fully stable mesophase. It melts directly from a pink crystal to a blue liquid crystal at 153 °C. Figures 4a−e show this transition taking place. The fluid nature of the mesophase is clearly evidenced by the droplet shapes of the blue regions, which are seen to flow and coalesce into larger droplets while the transformation proceeds. The black regions in these polarized micrographs are voids where no material is present. If the liquid crystal of **3** is cooled very slowly (less than one degree per minute), the pink crystal will reappear at about 105 °C. If, however, the sample is cooled more quickly, the liquid crystal texture will persist all the way down to room temperature and thus a liquid crystalline "glass" has been formed. Similar glasses have been observed for extended polymeric copper systems,[40] and it can be suggested that the bulky perchlorato counterions maximize the head-to-head distance favoring motions along the secondary lamellar arrangement of the interdigitated end-on alkyl chains. On heating, this glassy phase will convert to the crystal at about 105 °C and then convert back to the liquid crystalline phase at 153 °C.

After completing the above observations the sample was heated to observe the transition to the isotropic phase, which took place at 186 °C. This high temperature evidently produced some degradation of the sample, such that in subsequent measurements the lower transition temperatures were all shifted downward.

Differential Scanning Calorimetry. A selection of DSC measurements for **1**−**3** is shown in Figure 5. The first heating cycle performed on complex **1** showed that there is a small-entropy transition at 83 °C and then a more energetic transition, presumably melting to the isotropic transition, taking place at 134 °C. The 7 °C shift to higher temperature of this transition compared to microscopic studies may arise from the higher heating rate of the DSC (10 °C per minute). The DSC proceeded up to 160 °C, a higher temperature than that of the polarized optical microscopy experiments, thus altering permanently the sample as evidenced by the second heating cycle. A similar decomposition has been documented in the literature[41] and leads to six new and closely spaced peaks that appeared at lower temperatures. It is noteworthy that these peaks reappeared in identical form on the third heating cycle, thus indicating that they correspond to reproducible phase transitions. Although we are currently investigating the nature of these transitions, they bear no relationship to the 110 °C transition between liquid crystal and crystal that was observed by microscopy.

The first heating cycle performed on complex **2** showed a large peak at 152 °C followed by a small one at 166 °C. We presume that these most likely represent, respectively, melting to a mesophase followed by a transition to the isotropic phase. On the second heating cycle these two peaks have shifted to 136 and 148 °C with the larger of the two being considerably reduced in magnitude. On the third heating only one broad peak remained at 130 °C. Therefore, although there is indirect evidence of a stable high temperature mesophase, it is also clear that there is degradation of the sample with time and probably loss of stability of the mesophase. This may explain why in the microscope only one monotropic transition to the liquid crystal has been

(34) Prajapati, A. K.; Bonde, N. *Liq.Cryst.* **2006**, *33*, 1189.
(35) Szydlowska, J.; Jurkiewicz, A.; Krowczynski, A. *Liq. Cryst.* **2004**, *31*, 1655.
(36) Paschke, R.; Liebsch, S.; Tschierske, C.; Oakley, M. A.; Sinn, E. *Inorg. Chem.* **2003**, *42*, 8230.
(37) Hoshino, N.; Takahashi, K.; Sekiuchi, T.; Tanaka, H.; Matsunaga, Y. *Inorg. Chem.* **1998**, *37*, 882.
(38) Yelamaggad, C. V.; Hiremath, U. S.; Nagamani, S. A.; Rao, D. S. S.; Prasad, S. K.; Iyi, N.; Fujita, T. *Liq. Cryst.* **2003**, *30*, 681.
(39) Meyer, E.; Zucco, C.; Gallardo, H. *J. Mater. Chem.* **1998**, *8*, 1351.
(40) Caruso, U.; Panunzi, B.; Roviello, A.; Sirigu, A.; Spasiano, D. *J. Polym. Sci.* **2001**, *39A*, 2342.
(41) Liao, C.-T.; Wang, Y.-J.; Huang, C.-S.; Sheu, H.-S.; Lee, G.-H.; Lai, C. K. *Tetrahedron* **2007**, *63*, 12437.

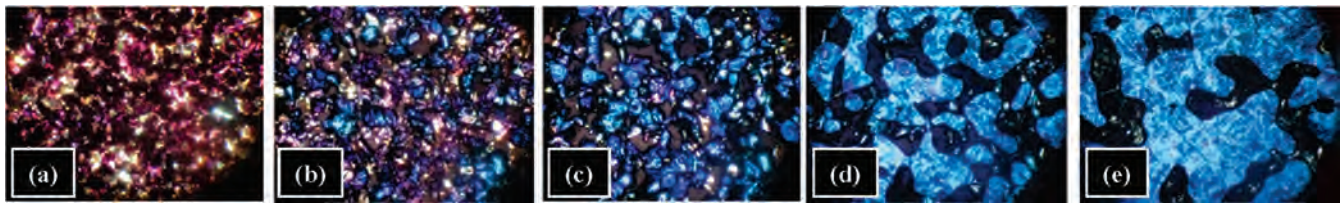

Figure 4. Micrographs of the liquid crystalline phases for **3** at (a) 105, (b) 125, (c) 135, (d) 145, and (e) 153 °C.

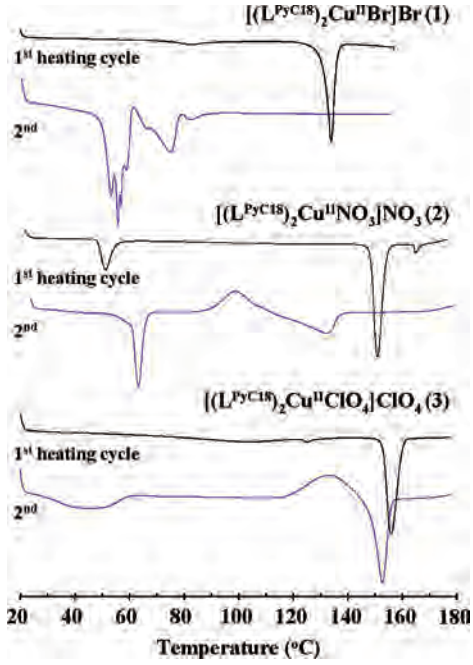

Figure 5. DSC measurements for **1**, **2**, and **3**. The heat flow axis ($W \cdot g^{-1}$) is omitted for clarity.

observed. At lower temperatures there was also a large exothermic peak appearing in the second and third heating cycles of **2**. This might result from the conversion of a glassy phase to a crystalline phase, as discussed above for **3**.

Complex **3** was the best behaved of this series of compounds. All three DSC measurements showed a prominent peak appearing at about 153 °C, exactly where the microscopic observations found the crystal to liquid crystal phase transition. On the second and third heating cycles there was a broad exothermic peak corresponding to the glass-to-crystal transition described above. To prevent degradation of the sample and ensure the observed reproducibility, these measurements did not reach sufficiently high temperatures to detect the transition to the isotropic phase appearing at 186 °C to prevent degradation of the sample and ensure the observed reproducibility.

X-Ray Diffraction of the Mesophases. X-ray measurements were performed at every 5 °C intervals while heating the samples. Because of ambiguity interpreting the initial results on **1**, its study was repeated using 2 °C increments. At room temperature, **1** has a sharp peak at a wave vector q of 0.24 $Å^{-1}$ corresponding to a periodicity of 26 Å, in excellent agreement with the single crystal results. At 135 °C intermediate-angle measurements display a new broad peak at $q = 0.18$ $Å^{-1}$ that increases in intensity until melting, which occurs at 143 °C. We interpret this peak as arising from a poorly ordered smectic phase, with a layer spacing of 35 Å, swollen about 35% compared to the crystal phase layer spacing. Intermediate-angle measurements on complex **2** revealed to have a peak at $q = 0.245$ $Å^{-1}$ indicating a spacing of 25.6 Å, again in excellent agreement with the single crystal results. At 150 °C an intense peak appeared at $q = 0.175$ $Å^{-1}$ and a weaker harmonic at 0.352 $Å^{-1}$, indicating a smectic phase with a layer spacing of 35.9 Å, thus about 40% larger than that of the crystal phase. Measurements in the wide-angle configuration were consistent, and showed no reflections at very wide angles, consistent with the assignment to a smectic mesophase rather than a lamellar crystal. For complex **3** in the intermediate apparatus a peak at $q = 0.245$ $Å^{-1}$ was observed at room temperature, again consistent with the single crystal results. At 165 °C a new peak appeared at $q = 0.168$ $Å^{-1}$ associated with a layer spacing of 37.4 Å and thus a 46% layer swelling. The wide angle measurement at 175 °C showed a peak at $q = 0.18$ $Å^{-1}$ and at its harmonic $q = 0.34$ $Å^{-1}$ yielding a slightly different layer spacing of 35.7 Å. Thus, it seems most plausible that the stable mesophase in this system is smectic.

The behavior of complexes **1**−**3** shows similarities and allows for a generalizing scenario for the series. At low temperatures the crystals of these compounds are bilayered structures having interdigitated alkyl tails. At higher temperatures the tails undergo rapid conformational changes, which is incompatible with the interdigitation. The chain motions force the layers to swell until the opposing alkyl chains are separated from each other and the mesophase is a monolayer smectic, most likely smectic A. A 40% swelling seems reasonable for this effect. Similarly, the nature of the apical ligand seems to control the stability of the mesophases, with perchlorates yielding the most stable mesophase.

Summary and Conclusions

In this article we have used a new pyridine-based ligand L^{PyC18} to develop copper-containing surfactants that exhibit mesomorphism. Because this ligand is an NN′ bidentate species, complexes of the type $[(L^{PyC18})_2Cu^{II}Y]Y$ result, where the fifth position of the metal center is occupied by an anionic ligand Y^- such as bromo for **1**, nitrato for **2**, and perchlorato for **3**. Structural information was obtained for **3**, as well as for **1** and **2** by means of model complexes **4** and **5** that exhibit a shorter tetradecyl chain. The nature of these apical ligands influences the mesogenic behavior of the resulting complexes, so that the smallest bromo-substituted species **1** shows a metastable liquid crystalline phase upon cooling at 110 °C. Moving in this series to a bulkier nitrato-substituted species, as in **2**, increases the transition temperature to 136 °C. The resulting mesophase

is still metastable. Finally, use of a bulky perchlorato species leads to well behaved mesophases for **3** at 153 °C. It can be concluded that the behavior of such metallomesogens is not trivial and will require further investigation that includes other apical ligands such as sulfates and acetates. Nonetheless, it seems particularly relevant that small changes in the geometry of cationic mesogens can be imposed by the presence of apically coordinated anions, allowing for tuning in the properties of the resulting mesophases. Conceptually it can be envisioned that the presence of such different anionic species dictates the dimension and order of channels and ridges in cationic mesogens. This phenomenon opens the possibility for the development of a new class of conductive materials where charge transfer may take place when an ordered thermotropic mesophase is present, and upon lowering of the temperature, generation of a randomly oriented solid leads to loss of conductivity. This hypothesis is currently under development in our laboratories.

Acknowledgment. C.N.V. thanks the Wayne State University, the Donors of the ACS-Petroleum Research Fund (Grant 42575-G3), the Nano@Wayne initiative (Fund-11E420), and the National Science Foundation (Grant CHE-0718470). P.A.H. acknowledges support by the MRSEC program of the National Science Foundation (Grant DMR05-20020). We thank Mr. L. Wu and Prof. Sandro da Rocha for the measurement of the DSC data.

Supporting Information Available: This material is available free of charge via the Internet at http://pubs.acs.org.

IC8005162